Renewable Energy 164 (2021) 1320–1333

Contents lists available at ScienceDirect

Renewable Energy

journal homepage: www.elsevier.com/locate/renene

A novel three-dimensional numerical model for PV/T water system in hot climate region

Tareq Salameh [a, *], Muhammad Tawalbeh [a], Adel Juaidi [b, **], Ramez Abdallah [b], Abdul-Kadir Hamid [c]

[a] Sustainable and Renewable Energy Engineering Department, University of Sharjah, P.O. Box 27272, Sharjah, United Arab Emirates
[b] Mechanical Engineering Department- Faculty of Engineering & Information Technology. An-Najah National University, P.O. Box 7, Nablus, Palestine
[c] Electrical Engineering Department, University of Sharjah, P.O. Box 27272, Sharjah, United Arab Emirates

ARTICLE INFO

Article history:
Received 13 May 2020
Received in revised form
24 October 2020
Accepted 30 October 2020
Available online 2 November 2020

Keywords:
PV/T
Novel numerical model
CFD model Simulation
PV cooling
Hot climate

ABSTRACT

Hybrid PV/Thermal systems (PV/T) are proposed to harvest the two renewable forms of solar energy, electrical and thermal. The use of PV/T systems improves electrical efficiency while utilizing the available solar thermal energy for various heating applications. In this work, numerical simulations perform for PV/T system in hot climate conditions. The cooling system consists of eleven channels arranged in parallel to each other on the backside of the PV module. A novel three-dimensional numerical model of the PV/T system was developed to evaluate the thermal efficiency. The standard k − epsilon model was used to simulate the flow. This novel system was based on using symmetric-convection boundary conditions for the right and left sides of the PV/T model and symmetric-symmetric boundary conditions for the middle cooling channels rather than simulating the whole cooling system. Using one channel simulation allows the creation of less number of meshes, hence, reduces the computational time. The thermal efficiency was estimated by the superposition method for all cooling channels of the PV/T system. The thermal efficiency of the PV/T system was 60% at 0.4 (L/min) and 68% at 5.4 (L/min). The obtained results were in good agreement with the results presented in the literature.

1. Introduction

The increased demand and consumption of fossil fuels led to their fast depletion along with the elevation of greenhouse gas emissions and consequently, global warming and climate change [1,2]. The utilization of renewable energy resources and/or the implementation of co-generation approaches are some favorable alternatives to fossil fuel consumption [3]. Solar energy, in particular, is not like conventional energy resources that have high environmental impacts. It is a renewable, abundant, and green source for a sustainable future [4–7].

Hybrid PV − Thermal (PV/T) systems that combined photovoltaic (PV) solar cells with solar thermal absorbers showed significant enhancements in capturing solar energy [8]. Both electrical and thermal energies are harvested from solar radiation using PV/T hybrid systems. Hence, in addition to, enhance the electrical efficiency of PV cells, the hybrid system of PV/T will also capture the thermal energy that can be utilized in various heating applications [9]. This is mainly because the increase in the PV cell temperature reduces the efficiency of PV cells dramatically [10]. Nevertheless, the implementation of the PV/T system allows the user to utilize the thermal energy [11].

Several techniques were used for PV cooling such as forced water circulation, forced air circulation, water spraying, water immersion, heat sink, phase change materials, transparent cooling, and thermoelectric cooling [12]. Water and air are the most commonly utilized cooling fluid in PV/T systems [13], where the PV/T system is named according to the cooling fluid utilized. For instance, PV/T/w and PV/T/a are the water and air-cooled PV/T systems, respectively. The selection of cooling fluid depends on several aspects and conditions. Using air as the cooling fluid is simple and cheaper and consequently, more economically feasible. However, it is not efficient in hot climates where air temperatures are above 20 °C [14]. On the other hand, using water is more efficient, yet, the cooling system would be more expensive when

* Corresponding author.
** Corresponding author.
E-mail addresses: tsalameh@sharjah.ac.ae (T. Salameh), adel@najah.edu (A. Juaidi).

https://doi.org/10.1016/j.renene.2020.10.137
0960-1481/

compared to the air [15,16]. The utilization of a nanofluid instead of water in a PVT system improves the performance and further enhances both electrical and thermal efficiencies [17]. Illustratively, Nasrin et al. [18] performed experimental and numerical studies for the enhancement of the efficiency of the PV/T system using nanofluid based on water/MWCNT for different irradiation and MWCT weight fractions. Their results showed that the overall efficiency at 1000 W/m^2 irradiance was improved and reached up 89.2%. PV/T systems can be classified in accordance with the fluid utilized for cooling, heat extraction type, system configuration arrangement, solar input type, and end-use purpose. Fig. 1 summarizes the various classification of PV/T systems [13].

United Arab Emirates (UAE) is located in the Arabian Peninsula which is recognized for the hot and sunny climate throughout the entire year [19]. This substantial exposure to solar radiation encourages the country to promote photovoltaic technology for electricity generation [20,21]. PV systems are more environmentally friendly compared to other renewable energy technologies with no significant operational pollution [22–24] and they require less operating and maintenance costs [25]. The UAE is one of the highest worldwide countries in electricity consumption, where the total annual electrical production for Abu Dhabi Water and Electricity Authority (ADWEA) and Dubai Water and Electricity Authority (DEWA) was approximately 123.0 TWh and the per capita consumption was around 13.1 MWh [26]. Despite the abundance of oil in UAE, the country's vision is to include renewable energy and nuclear energy in its energy mix [27]. The UAE is progressing substantially in achieving its goal by installing several solar power plants such as SHAMS solar power plant and Mohammed Bin Rashed solar park [28]. Nevertheless, the UAE hot and dusty weather depresses the performance of solar power systems. For instance, elevated temperatures [29,30], as well as the accumulation of dust [31,32], negatively affect the performance of various generations of PV cells. Consequently, the implementation of solar PV systems in UAE is problematic without proper cooling and cleaning.

Nowadays, the electrical efficiency of commercial PV panels ranges from 10 to 25% [33]. This means 75–90% of the solar radiation falls on a PV module is either reflected or dissipated as thermal energy. The latter leads to decreasing the open-circuit voltage and the fill factor of the module due to the increase in the PV module temperature, hence, decreases the PV module electrical efficiency [34]. Currently, the most employed PV cells are the monocrystalline silicon (mono c-Si) and the polycrystalline Silicon (poly c-Si) [35]. The efficiencies of these types are strongly affected by the increase of the panel temperature [34–38], with a temperature coefficient between − 0.45 and − 0.50% [39]. However, the effect of temperature on the amorphous silicon cells is significantly lower, with a temperature coefficient of about − 0.25% [40].

Numerous numerical and experimental research investigations have been performed recently to study, the effect of variation of temperature, irradiation, wind speed, and mass flow rate of the cooling fluid on the efficiencies of PV/T systems [41–44]. These studies focused mainly on the overall efficiency of the system, i.e. electrical and thermal efficiencies, and on identifying the PV/T system that possesses the best performance and the lowest cost. Few studies [43,45–47] examined the use of the three-dimensional simulation for the whole PV/T system. The results of these studies revealed that the thermal efficiency seems to vary with the shape of the cooling collector, area of PV module, solar irradiance, fluid cooling temperature, overall heat transfer coefficient, specific heat, and mass flow rate of cooling fluid.

The novel numerical model used in this study is based on simulating one cooling channel instead of simulating the whole PV/T system as reported in other numerical simulations in the literature. The simulations were performed in this model three times, one time for a cooling channel in the middle of the PV/T system, one time for the channel on the left side, and one time for the channel on the right side of the PV/T system. This was achieved by applying symmetric-symmetric thermal boundary conditions for the channel in the middle and symmetric-convection thermal boundary conditions for the channels on the left and right sides. It is worthwhile to mention that the numerical simulations performed for the whole PV/T system require a very high number of elements and consume more computational time. For instance, the numbers of elements used by Nasrin et al. [43], Pang et al. [45], and Misha et al. [46] were 1,434,582, 3,262,009, and 2,432,207, respectively. These are 5–12 times higher than the number of elements used in

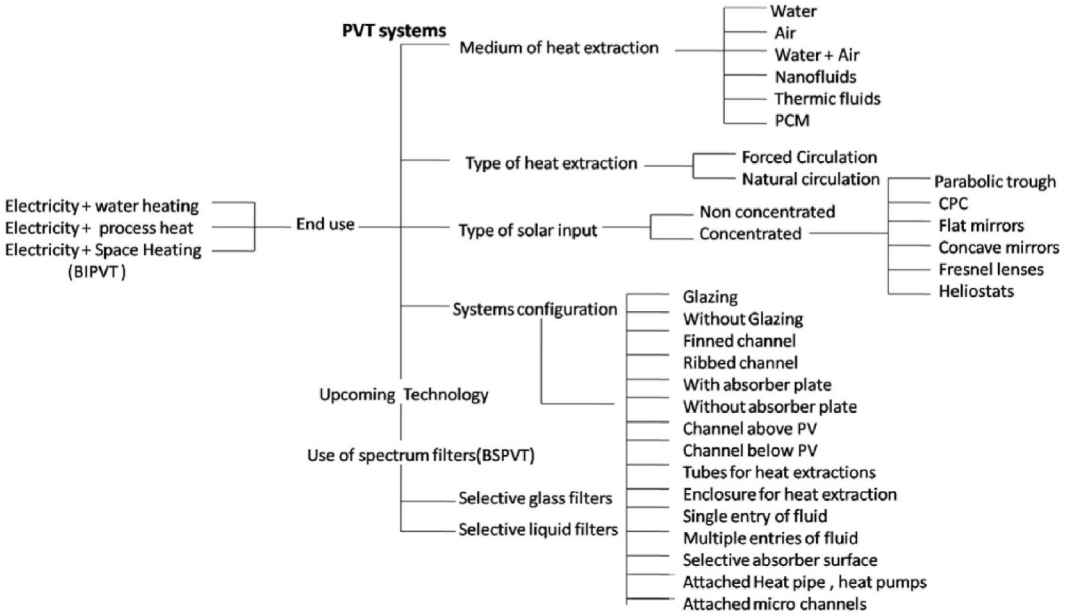

Fig. 1. Classification of PV/T systems [13].

this study which was 270,000 elements with a computational time of only 7 min. This study aims at numerically studying the performance of a PV/T system using a novel three-dimensional model under real conditions of irradiance and temperature for Sharjah city, UAE as a semi-arid climate with hot summer and mild winter.

2. Methodology

2.1. Electrical part

The PV module based on polycrystalline silicon was used, the electrical features of this PV module are shown in [48]. The maximum power point (P_{MPP}) produced by a solar PV system is calculated by Eq. (1):

$$\dot{Q}_{MPP} = P_{MPP} = I_{MPP} V_{MPP} = (FF) V_{oc} I_{sc} \tag{1}$$

where I_{MPP} and V_{MPP} are the current and the voltage at the maximum power point, respectively, and *FF* is the fill factor that varies from one cell to another. This variation is based on the quality of the material used in the cell (purity of silicon). Moreover, the open-circuit voltage and the short circuit current are V_{oc} and I_{sc}, respectively. The electrical efficiency (η_{elec}) of the PV module is determined using Eq. (2):

$$\eta_{elec} = \frac{I_{MPP} V_{MPP}}{GA} \tag{2}$$

where *A* is the area of the PV module (1.17 m × 0.67 m), and *G* is the irradiance or the solar radiation in (W/m^2). The value of *MPP* varies from one location to another based on the ambient temperature and irradiance. The effect of the temperature on the *MPP* is given by temperature coefficients for current, voltage, and power. The electrical characteristics of the PV module under different conditions are calculated based on the aforementioned coefficients and the electrical characteristics under standard test conditions (STC) of the PV module. However, the electrical efficiency of the PV module under the effect of the temperature is shown in Eq. (3) [34].

$$\eta_{elec} = \eta_{ref} \left[1 - \beta_{ref} \left(T - T_{ref} \right) \right] \tag{3}$$

where the η_{ref} is the efficiency at reference temperature, β_{ref} is the temperature coefficient for the electrical efficiency, *T* is the temperature under actual operating condition (- 40–85 °C) and T_{ref} is the reference temperature under STC (25 °C). This drop in efficiency can be reduced by using a suitable cooling system to keep the solar module operating close to the SOC.

2.2. Thermal part

The rate of heat removal ($\dot{Q}_{th}$) by the cooling system can be calculated as follows:

$$\dot{Q}_{th} = \dot{m}_{water} C_p (T_{outlet} - T_{inlet}) \tag{4}$$

where $\dot{m}_{water}$, T_{outlet}, T_{inlet}, and C_p are the mass flow rate, outlet temperature, inlet temperature, and specific heat of the cooling water, respectively. The inlet temperatures were recorded at different values of irradiance and. Moreover, the rate of the useful thermal energy ($\dot{Q}u$) is the difference between the rates of absorbed radiation and heat losses and is given by Eq. (5):

$$\dot{Q}_u = A_c \left[G - U_L (T_{p,m} - T_a) \right] \tag{5}$$

where A_c is the surface area of the collector, U_L is the overall loss heat transfer coefficient. $T_{p,m}$, and T_a are plate mean temperature and ambient temperature, respectively. However, because of the difficulty in measuring $T_{p,m}$, Eq. (5) was modified by Hottel and Wilhier [49] to be:

$$\dot{Q}_u = A_c F_R \left[G - U_L (T_{p,m} - T_a) \right] \tag{6}$$

where F_R is the removal factor and it varies with the incident solar radiation, collector shape design, and fluid operating condition as shown in Eq. (7):

$$F_R = \frac{\dot{m} C_P}{A_c U_L} \left[1 - e^{\left(\frac{A_c U_L F'}{\dot{m} C_P} \right)} \right] \tag{7}$$

Where F' is the collector efficiency factor. Moreover, the thermal efficiency of the PV/T system (η_{th}) is calculated based on the rate of thermal energy extracted from the PV module as shown in Eq. (8):

$$\eta_{th} = \frac{\dot{Q}_{th}}{GA} \tag{8}$$

Finally, the overall efficiency is the sum of thermal efficiency and electrical efficiency of the PV/T system (η_o) and is calculated as follow:

$$\eta_o = \eta_{th} + \eta_{elec} \tag{9}$$

One way to improve the efficiency of the PV/T system is to couple it with other heat users such as driving a heat pump. This would convert solar energy into useful heat more efficiently and increase the working fluid temperature from the combined system significantly, hence, improve the overall utilization efficiency of solar energy [50]. However, the coupling adds to the complexity of the system and requires additional management due to the instability and intermittency nature of solar energy. For instance, during the summer season, the thermal energy produced from the combined system could be used to heat the domestic hot water supply, while during the winter season an auxiliary heater could be utilized to provide the desired thermal energy. Moreover, to attain a steady heating system, the system should be combined with a built-in thermal energy storage system such as a reversible thermochemical reaction or a phase change material [51]. However, adapting a thermal energy storage system raises the cost of the system and introduces more constraints for the system location, therefore, affects the feasibility of the whole system [52]. Furthermore, to obtain a more accurate estimate of the PV/T efficiency the calculations should be corrected by considering the effect of soiling, energy losses in wires and converters, and heat losses in the hydraulic loop [52].

2.3. Experimental setup and uncertainty

The PV/T system consists of a PV module and a thermal system, the specifications of these systems are presented in Table 1.

The IV and power curves at different irradiance for the PV module were measured by PROFITESTPV. The thermal energy for PV/T system was calculated at different irradiance by measuring the mass flow and the inlet and outlet temperatures of the cooling channel as presented in Eq. (4). The relative uncertainty for electrical and thermal efficiency were both estimated based on the uncertainty associated with the measuring instruments used in the experimental setup as shown in Table 2. The absolute uncertainties for measurement parameters were estimated based on the instrument device uncertainty and the repetition uncertainty for the

Table 1
PV/T system specifications.

PV/T Components	Specification
PV	Poly-crystalline Si
P_{max} at STC	100 W
V_{mp}	18 V
I_{mp}	5.55 A
V_{oc}	21.24 V
I_{sc}	6,11 A
Operating temperature	- 40 to 85 °C
Weight	7.1 kg
Module dimensions	1.17 m × 0.67 m × 0.03 m
Thermal system	
Pump power (DC)	5 W
Pump flow rate	5.4 L/min
Channel material	Copper
Number of channels	11
Channel dimensions	0.0127 m × 0.00635 m
Temperature sensors	- 50 to 250 °C
Storage system	
Battery	12 V

Table 3
Relative Uncertainties for irradiance, electrical and thermal efficiencies.

$\delta G/G$	$\delta\eta_{elec.}/\eta_{elec.}$	$\delta\eta_{th.}/\eta_{th.}$
$f(G)$	$f(G, P_{MPP.})$	$f(G, \dot{m}_{water}, T_{outlet}, T_{inlet})$
From measurement	From Eq. (2)	From Eqs. (4) and (8)
±0.0057	±0.014	±0.02

Table 4 shows the physical and thermal properties details of the PV module utilized in these simulations [54].

Fig. 2 shows the steady-state energy balance for the PV/T system used in this study. The general form for energy balance can be presented as in Eq. (14).

$$\frac{dQ}{dt} = \dot{Q}_{in} - \dot{Q}_{out} \tag{14}$$

For steady state condition, the previous energy balance equation becomes.

Table 2
Absolute uncertainties for the instrument device and the measured parameter. If R is considered as any function of independent linear parameters as in Eq. (11).

$$R = f(p_1, p_2, p_3, \ldots p_n) \tag{11}$$

Instrument device	Measurement variable	Uncertainty	
		Instrument device	Maximum measured
PROFITESTPV (Germany)	Solar irradiance	±10 W/m^2 for (T_{cell} ± 1 K)	4 W/m^2
PROFITESTPV (Germany)	Peak power	±5 W	1 W
Thermocouple type K	Ambient temperature	±0.5 °C	0.3 °C
TM700 Thermocouple Thermometer	Cooling fluid temperature	0.1–0.3 °C	0.2 °C
VYAIR 2.4 to 60.0 litres/min DigiFlow 6710M-66 Digital Micro Flow	Mass flow of cooling fluid	0.04–0.54 L/min	0.1 L/min

measured parameter as shown in Eq. (10).

$$\delta p = \sqrt{(\delta p_{dev})^2 + \left(\delta p_{rep}\right)^2} \tag{10}$$

where δp_{dev} and δp_{rep} are the device and repetition uncertainties for the measured parameter, respectively.

Then the absolute uncertainty of function R can be calculated as follows [53]:

$$\delta R = \sqrt{\left(\frac{\partial R}{\partial p_1}\partial p_1\right)^2 + \left(\frac{\partial R}{\partial p_2}\partial p_2\right)^2 + \ldots + \left(\frac{\partial R}{\partial p_n}\partial p_n\right)^2} \tag{12}$$

where n is the total number of measured parameters. If the uncertainties of the parameters are independent and the absolute uncertainty divided by the function R, then the absolute uncertainty is converted to relative (fractional) uncertainty as shown in Eq. (13).

$$\frac{\delta R}{R} = \sqrt{\left(\frac{\partial p_1}{p_1}\right)^2 + \left(\frac{\partial p_2}{p_2}\right)^2 + \ldots + \left(\frac{\partial p_n}{p_n}\right)^2} \tag{13}$$

Based on Eq. (13), the uncertainties for electrical and thermal efficiencies were calculated from Eqs. (2), (4) and (8) and the values are shown in Table 3.

2.4. Numerical modeling and simulations

3-Dimensional (3-D) numerical simulations were utilized to compute the thermal and hydraulic behaviors of the PV/T system.

$$\dot{Q}_{in} = \dot{Q}_{out} + \dot{Q}_{in} = \dot{Q}_{elec} + \dot{Q}_{th} + \dot{Q}_{loss} \tag{15}$$

where $\dot{Q}_{in}$ is the incidence solar irradiance (AG) on the top surface of the PV/T system, $\dot{Q}_{loss}$ is the rate of heat losses from the PV/T system by convection and radiation which are calculated by Eqs. (16) and (17), respectively.

$$\dot{Q}_{conv} = h\, A_c\, (T_{p,m} - T_a) \tag{16}$$

$$\dot{Q}_{rad} = \sigma\varepsilon\left(T_{p,m} + T_{Sky}\right)\left(T_{p,m}{}^2 + T_{Sky}{}^2\right)A_c\left(T_{p,m} - T_{sky}\right) \tag{17}$$

where h is the heat transfer coefficient in (W/m^2.K), for this condition, h was used based on the approximation proposed by Watmuff et al., 1977 [55].

$$h = 2.8 + 3 \times V \tag{18}$$

where V is the speed of wind in (m/s). This approximation is used after considering the variation on the speed is less than 4 (m/s). σ is Stefan Boltzmann constant which equal to 5.67 × 10^{-8} W/m^2.K^4, ε is the emissivity of the PV/T surface and $T_{Sky} = 0.0552T_a^{1.5}$ is the sky temperature [43]. The solar PV system was cooled from the backside, the copper channel dimensions are 0.0127 m × 0.00635 m.

2.4.1. Geometry and mesh

The geometry was created in 3-D by DesignModeler software inside ANSYS 15. The geometry was split into several control

Table 4
Structural details of the PV module used in the simulations [54].

Layer #	Layer name	Thickness (m)	Density (kg/m^3)	Specific heat capacity (J/kg.K)	Thermal conductivity (W/m.K)
1	ARC	100×10^{-9}	2400	691	32
2	Glass	3×10^{-3}	3000	500	1.8
3	EVA	500×10^{-6}	960	290	0.35
4	PV Cells	225×10^{-6}	2330	677	148
5	Rear contact	10×10^{-6}	2700	900	237
6	Tedlar	10×10^{-5}	1200	1250	0.2

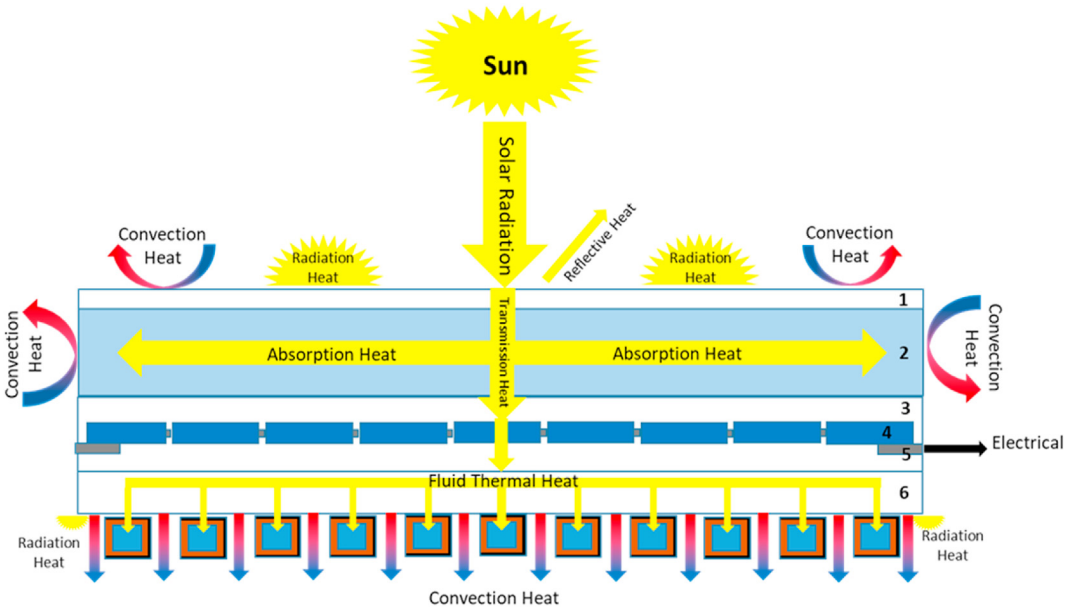

Fig. 2. The energy balance for a PV/T system consists of eleven copper cooling channels.

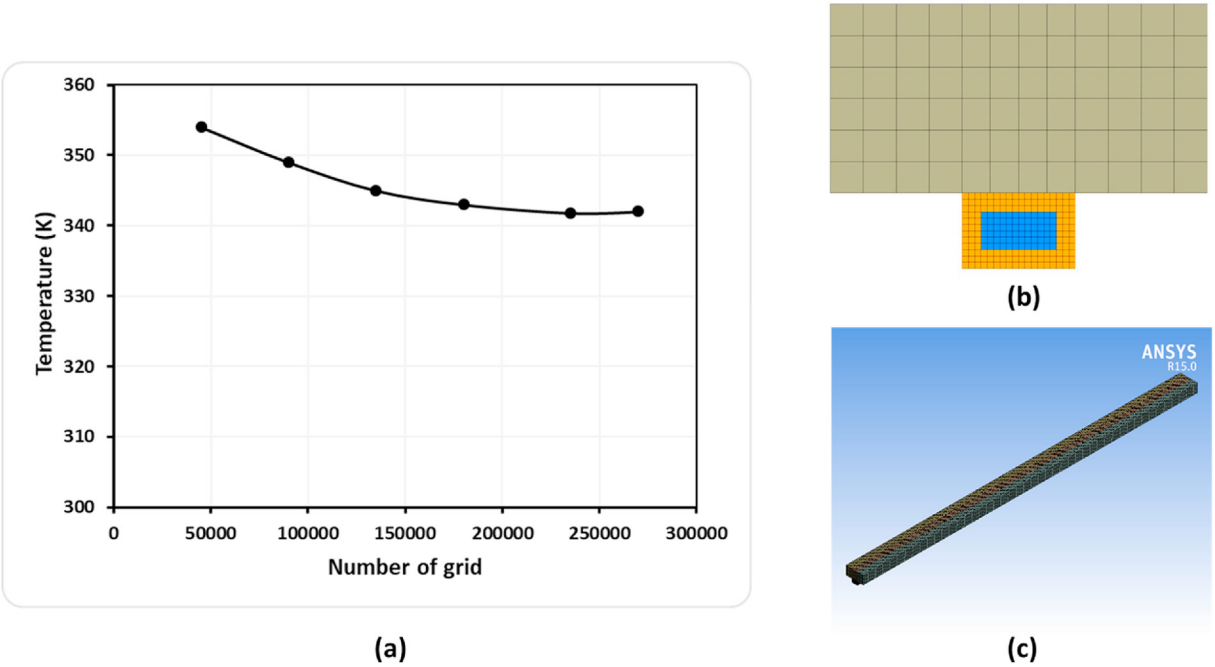

Fig. 3. **(a)** Effect of the number of grids on the temperature at the top of PV module **(b)** Cross section along the stream wise direction with hexahedral elements shapes for PV/T model **(c)** Computational domain of the PV/T numerical model with a copper cooling channel at the bottom with 270,000 hexahedral elements.

volumes to solve for conservation equations. The hexahedral shaped elements were used for simulations because it has a high aspect ratio as shown in Fig. 3. The mesh size was selected based on grid independent study. The mesh size was refined for the fluid flow inside the cooling channel, the size was 0.00071 m. However, the size for the mesh inside the PV module was 0.0032 m as shown in Fig. 3. Different numbers of grids were tested and the average temperature at the middle of the top surface was selected for the grid independent study as shown in Fig. 3. The numerical uncertainty in the fine-grid for this CFD simulation was estimated by 2.37% based on the study done by [56]. In order to reduce the time of computational and achieve the convergence quickly, only one cooling channel out of eleven channels is considered in the numerical simulation instead to discretized the whole geometry of the PV/T system (PV module and the thermal system which consist from eleven copper cooling channels).

2.4.2. Physical properties and boundary conditions

The equivalent thermo-physical properties for the structural details of the PV module were used as in [57] after assumed the PV module one homogeneous unit. The values of these thermo-physical properties were based on the information displayed in Table 4 and Fig. 2, while the thermo-physical properties for copper channels and the working fluid were used from the ANSYS Fluent database. The solar irradiance received the top surface of the computational domain was treated as constant heat flux after considering the product of solar transmissivity and solar absorptivity ($\tau\alpha$) of the PV module 0.9 [58], these values of heat flux were 900 W/m^2, 700 W/m^2, and 550 W/m^2 at different times of a typical day in April as shown in [48]. Both inlet and outlet boundary conditions were applied to the inlet and outlet positions of the copper cooling channel, respectively; four inlet water velocity values were simulated based on 0.4, 1.4, 3.4, and 5.4 (L/min) as the total mass flow rate in all eleven channels.

The convective heat transfer boundary condition was applied at the upper and lower side edges of the PV/T numerical model, as well as at the bottom side of the PV/T numerical model (PV module part) as shown in Fig. 4. Two different thermal boundary conditions were applied on both sides (left and right) of the PV/T numerical model based on the position of the cooling channel as mentioned before. The symmetric boundary condition was used for the cooling channel located in the middle of the PV module, while both symmetric and convective thermal boundaries condition were used for the cooling channel located at the left and right sides of the PV module. It is worth mentioning that the insulation thermal condition was applied to the copper cooling channel walls. The details of the boundary conditions for each type of PV/T model are presented in Table 5 and Fig. 4.

2.4.3. Governing equations and mathematical model

ANSYS Fluent was used the finite volume method to solve the steady-state governing equations for the PV/T numerical model as shown in Table 6.

G_k is the generation of turbulence kinetic energy due to the mean velocity gradients and is given by Eq. (19).

$$G_k = -\rho\overline{u_i'u_j'}\frac{\partial u_j}{\partial x_i} \tag{19}$$

The variables σ_k and σ_ε are the turbulent Prandtl numbers for k and ε. $C_{1\varepsilon}$ and $C_{2\varepsilon}$ are constants. The values of σ_k, σ_ε, $C_{1\varepsilon}$, and $C_{2\varepsilon}$ were 1, 1.3, 1.44, and 1.92, respectively. The turbulent viscosity is calculated by combining k and ε as in Eq. (20).

$$\mu_t = \rho C_\mu \frac{k^2}{\varepsilon} \tag{20}$$

The modeling constants C_μ value is 0.09. Both mass and Navier–Stokes equations were used to solve the incompressible flow field for the k-ε turbulence model inside the copper cooling channel, while the energy equation was used to solve the temperature fields for the flow field inside the copper cooling channel, copper channel walls and the PV module. The convergence criteria for mass, momentum, and energy equations were 10^{-4}, 10^{-6}, and 10^{-7}, respectively, these convergence criteria achieved after 7 min. The outlet temperature was evaluated based on the area average weight of the outlet of the cooling channel as shown in Eq. (21).

$$T_{out} = \frac{1}{T_{out}}\int T_{out}dA \tag{21}$$

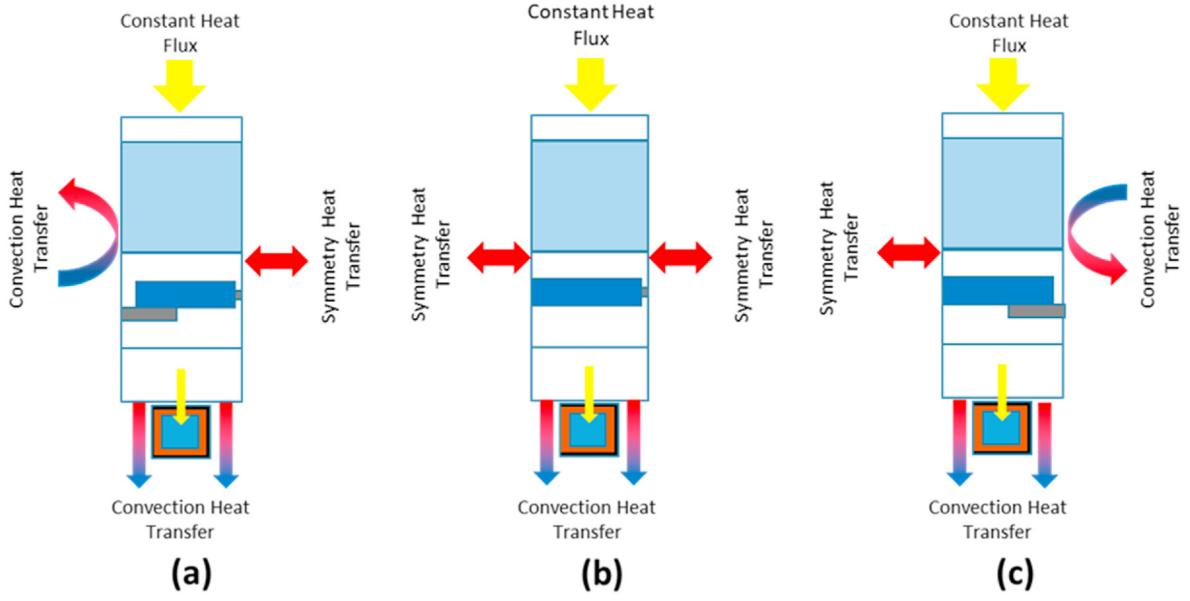

Fig. 4. Boundary conditions for three different locations of PV/T model (a) left (b) middle (c) right.

Table 5
Type of boundary condition for three different locations of PV/T numerical model.

Location of PV/T system	Type of boundary condition for different locations of PV/T numerical model		
	Right side	Middle	Left side
Top of PV module	Constant heat flux (500, 700, and 900 W/m^2)	Constant heat flux (500, 700, and 900 W/m^2)	Constant heat flux (500, 700, and 900 W/m^2)
Right side of PV module	Convection heat transfer	Symmetry	Symmetry
Left side of PV module	Symmetry	Symmetry	Convection heat transfer
Bottom side of PV module	Convection and radiation heat transfer	Convection and radiation heat transfer	Convection and radiation heat transfer
Upper side edge of PV module	Convection and radiation heat transfer	Convection and radiation heat transfer	Convection and radiation heat transfer
Lower side edge of PV module	Convection and radiation heat transfer	Convection and radiation heat transfer	Convection and radiation heat transfer
Inlet of copper channel	Constant velocity temperature, kinetic energy and dissipation rate	Constant velocity temperature, kinetic energy and dissipation rate	Constant velocity temperature, kinetic energy and dissipation rate
Outlet of copper channel	Pressure outlet	Pressure outlet	Pressure outlet
Inner walls of copper channel	No slip for velocity Convection for temperature	No slip for velocity Convection for temperature	No slip for velocity Convection for temperature
Outer wall of copper channel	Thermal insulation	Thermal insulation	Thermal insulation

Table 6
Steady-state governing equations for the k-ε turbulence model.

$$\left\{\frac{\partial}{\partial x}(\rho u \varnothing)+\frac{\partial}{\partial y}(\rho v \varnothing)+\frac{\partial}{\partial z}(\rho w \varnothing)\right\}=\frac{\partial}{\partial x}\left(\Gamma_{\varnothing}\frac{\partial \varnothing}{\partial x}\right)+\frac{\partial}{\partial y}\left(\Gamma_{\varnothing}\frac{\partial \varnothing}{\partial y}\right)+\frac{\partial}{\partial z}\left(\Gamma_{\varnothing}\frac{\partial \varnothing}{\partial z}\right)+S_{\varnothing}$$

Equation	$\varnothing$	$\Gamma_{\varnothing}$	$S_{\varnothing}$
Continuity	1	0	0
U momentum	u	$\mu+\mu_t$	$-\frac{\partial p}{\partial x}+\frac{\partial}{\partial x}\left(\Gamma_{\varnothing}\frac{\partial u}{\partial x}\right)+\frac{\partial}{\partial y}\left(\Gamma_{\varnothing}\frac{\partial v}{\partial x}\right)+\frac{\partial}{\partial z}\left(\Gamma_{\varnothing}\frac{\partial w}{\partial x}\right)$
V momentum	v	$\mu+\mu_t$	$-\frac{\partial p}{\partial y}+\frac{\partial}{\partial x}\left(\Gamma_{\varnothing}\frac{\partial u}{\partial y}\right)+\frac{\partial}{\partial y}\left(\Gamma_{\varnothing}\frac{\partial v}{\partial y}\right)+\frac{\partial}{\partial z}\left(\Gamma_{\varnothing}\frac{\partial w}{\partial y}\right)$
W momentum	w	$\mu+\mu_t$	$-\frac{\partial p}{\partial z}+\frac{\partial}{\partial x}\left(\Gamma_{\varnothing}\frac{\partial u}{\partial z}\right)+\frac{\partial}{\partial y}\left(\Gamma_{\varnothing}\frac{\partial v}{\partial z}\right)+\frac{\partial}{\partial z}\left(\Gamma_{\varnothing}\frac{\partial w}{\partial z}\right)$
Temperature	T	$\mu/Pr+\mu_t/Pr_t$	0
Turbulent kinetic energy	k	$\mu+\mu_t/\sigma_k$	$G_k-\rho\varepsilon$
Dissipation rate	ε	$\mu+\mu_t/\sigma_{\varepsilon}$	$C_{1\varepsilon}\frac{\varepsilon}{k}G_k-\rho C_{2\varepsilon}\frac{\varepsilon^2}{k}$

After the outlet temperature of cooling fluid was evaluated, Eq. (4) was used to calculate the thermal energy for the PV/T numerical model for the two cooling channels at the right and left (symmetric-convection) as well as the nine cooling channels at the middle (symmetric-symmetric) of PV/T system. Fig. 5 shows the diagram for all procedures needed for the CFD of the PV/T system numerical simulations in this study.

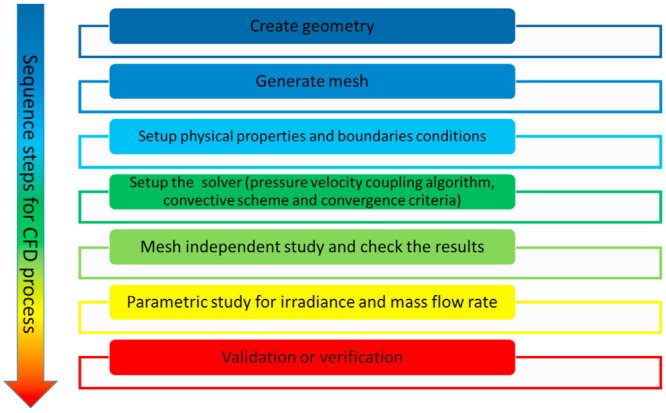

Fig. 5. The methodology adopted for numerical simulations of the PV/T system using ANSYS Fluent.

3. Results and discussion

3.1. Weather conditions

Fig. 6 (a) and (b) display the ambient temperature, cell temperature, and the irradiance for both PV and PV/T modules during a typical day in April for Sharjah city in UAE. All the temperature curves in Fig. 6 (a) follow the natural distribution of the ambient temperature during daylight. These three temperatures increase with time and reach a maximum values at around noon. These maximum temperature values for both PV/T and PV modules are 45 and 58 °C, respectively, at maximum ambient temperature of 40 °C. Then the temperatures decrease gradually until sunset. On the other hand, Fig. 6 (b) shows that the irradiance for both PV and PV/T modules reaches maximum values of 916 and 898 W/m^2, respectively, at the solar noon.

3.2. Electrical characteristic for the PV and PV/T systems

The electrical characteristics of the PV and the PV/T systems were measured using the profiTest PV analyzer device under three values of irradiance namely at 12:30 PM (900 W/m^2) as shown in Fig. 7 (a). It is clear from this figure that the PV/T module has a higher open-circuit voltage value of 20.34 V compared to the PV module value of 19.12 V. Whereas the values for the short circuit current were 6.25 A and 6.11 A for the PV/T and PV modules,

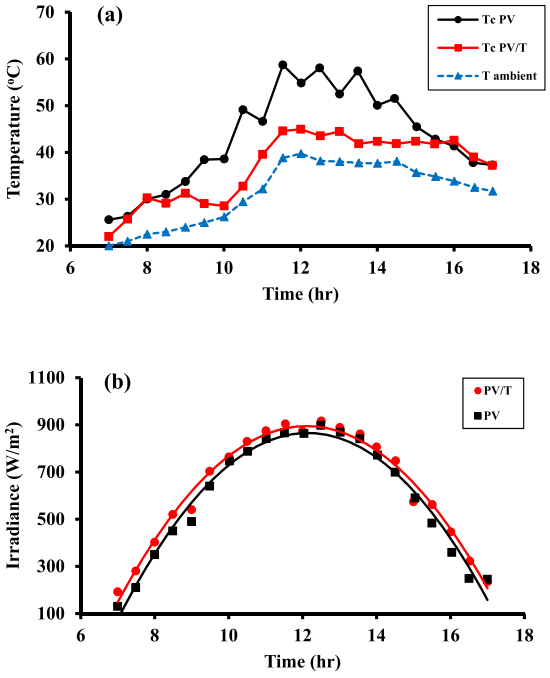

Fig. 6. The measuring parameters for PV and PV/T modules during a typical day of April in UAE **(a)** Ambient temperature and cell temperatures for PV and PV/T **(b)** Irradiance falls on PV and PV/T modules.

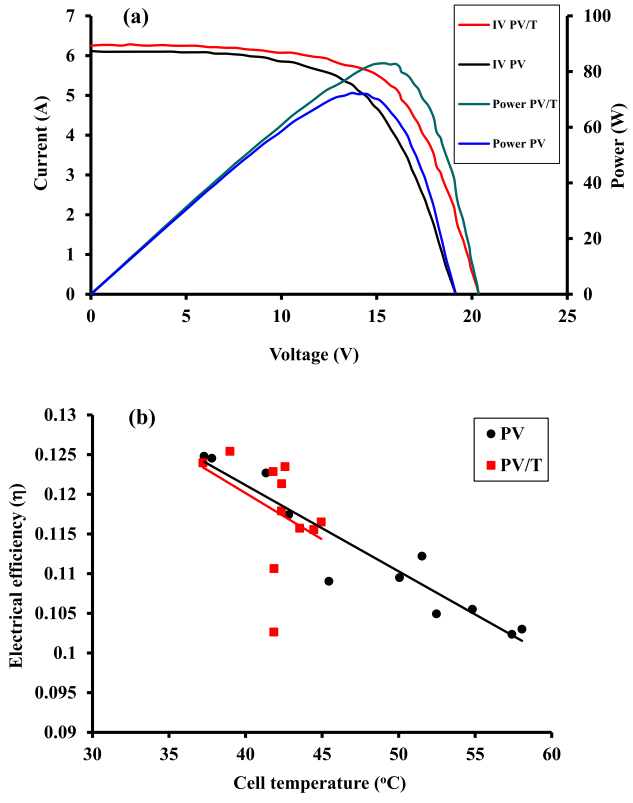

Fig. 7. The electrical performance for PV and PV/T system during a typical day in April in UAE **(a)** The IV and power curves **(b)** Electrical efficiency.

respectively. The PV/T module shows a maximum power point (MPP) value of 82.97 W, the MPP for the PV/T is higher than the value of MPP for the PV module by 10 W. Fig. 6 shows the measurements of electrical efficiencies for the PV/T and PV modules under different values of irradiance measured on the same working day in April. These efficiencies decrease linearly as the PV cell temperature increases as illustrated in Fig. 7 (b). It is evident from Fig. 6 that the minimum and maximum measurement electrical efficiencies for the PV/T module were 10.26% and 12.5%, respectively. On the other hand, the minimum and maximum measurement electrical efficiencies for the PV module were 10.23% and 12.5, respectively. It is clear that there was no difference between the upper and lower limits of the electrical efficiencies and that is mainly due to the narrow range of the cell temperatures of the PV/T module (37.22–44.95 °C). This makes the cooling system for the PV/T module more effective compared to the PV module without the cooling where the cell temperature ranges between 37.3 and 58.06 °C. This difference in cell temperature causes the 10 W increase in the MPP as aforementioned. The drop in the cell temperature enhances electrical efficiency, especially under hot climate weather conditions. In other words, the cell temperature for the PV/T was very close to the nominal operating cell temperature (NOCT) or the standard operating conditions (SOC), which allows the PV/T system to operate at a higher electrical efficiency compared to the PV system. The latter works at a cell temperature far away from the SOC temperature. The cooling system extracted the waste heat during the energy conversion process. Furthermore, the cooling system will enhance the overall efficiency of PV/T by recovery this wasted thermal energy and make the system more sustainable.

3.3. Thermal characteristics of the PV/T system

3.3.1. Two-dimensional temperature distribution

The two-dimensional temperature distribution for PV/T system along the cooling channel (at the inlet, middle, and outlet positions) is displayed in Fig. 8. As shown in Fig. 8 (a), the value of the highest temperature was 342 K which was observed on the top surface in the middle of the PV/T module. This was when the symmetrical boundary condition applied on both sides in the numerical model. However, the lowest temperature was 311 K and it was at the inlet of the cooling channel. The temperature on the top surface of the PV/T module for the symmetrical boundary condition decreases along the cooling channel from inlet to outlet. The range of the temperatures on the top surface were 311–330.1 K, 313.4–342 K, and 315.8–334.8 K for the inlet, middle, and outlet location of the cooling channel, respectively. While Fig. 8 (b) and (c) show the two-dimensional temperature distribution when the symmetrical and convective boundaries conditions applied on both sides of the numerical model. The highest temperature was 337.9 K and it was observed in the middle of the PV/T module. The value of temperature for this boundary condition is lower than the value when the symmetrical thermal boundary condition applied on both sides of the numerical model. By similarity with symmetrical boundary conditions, the temperature at the top side of the PV/T module decreases along the cooling channel from inlet to outlet. The ranges of temperature in the inlet, middle, and outlet locations on the top surface were 311–327.6 K, 311–337.9 K, and 311–329.6 K, respectively. Fig. 8 (a), (b), and (c) show also that the top side of the PV/T module has the highest value of the temperature where the constant heat flux is applied, this value decreases to the lowest value when reaches the bottom of the copper channel of the cooling system.

3.3.2. Useful thermal energy from the PV/T system

Fig. 9 (a) shows the useful thermal energy of the PV/T that was absorbed by water under different values of irradiance (550, 700, and 900 W/m^2). The absorbed thermal energy increases as both irradiance and mass flow rates increase from 500 to 900 W/m^2 and

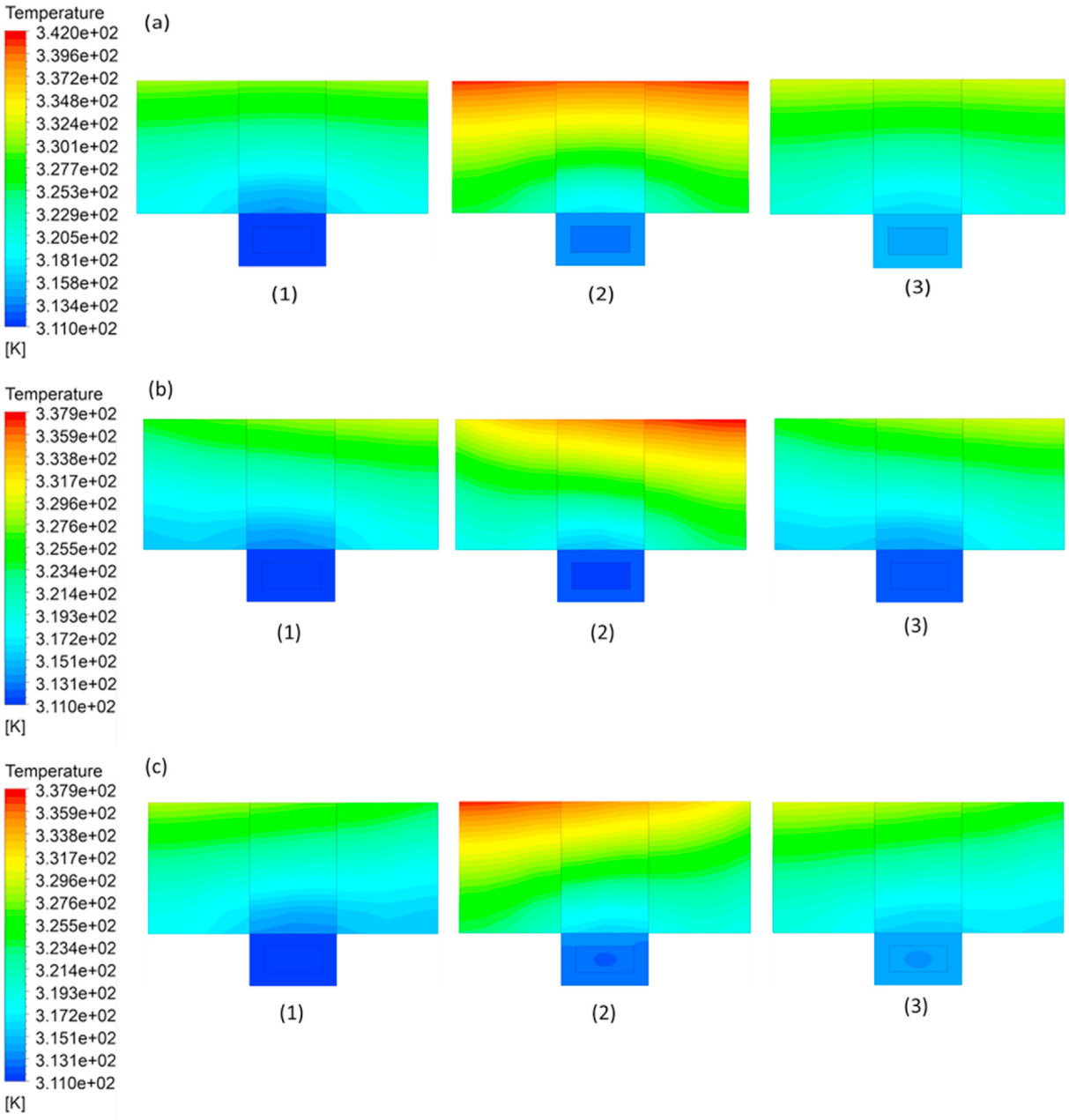

Fig. 8. Temperature contour plot for different boundary condition **(a)** symmetric-symmetric along the middle of PV module length **(b)** symmetric-convection conditions along the right edge of the PV module length **(c)** symmetric-convection conditions along the left edge of the PV module length at different location (1) inlet (2) middle (3) outlet.

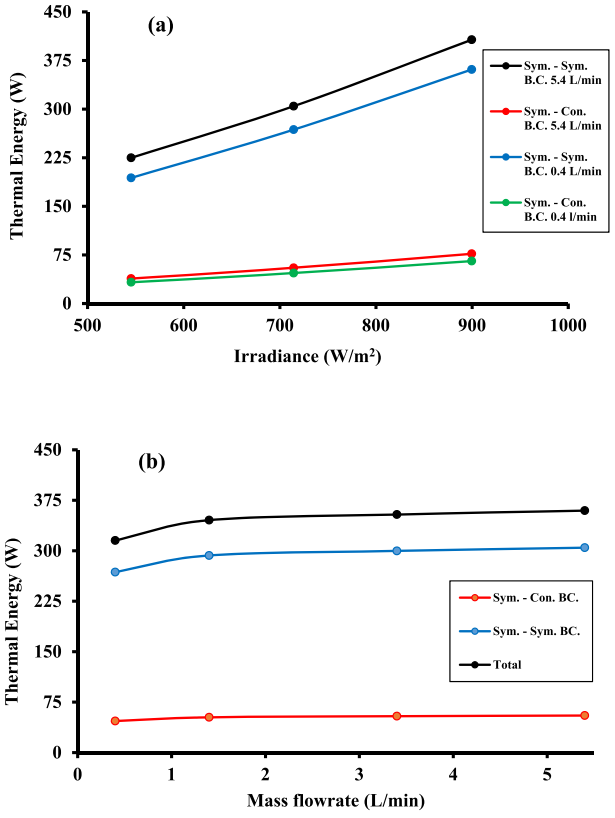

Fig. 9. Thermal energy under different thermal boundary conditions **(a)** different irradiance values along the day **(b)** different mass flow rates values at 700 W/m^2.

from 0.4 to 5.4 L/min, respectively. Corresponding to what mentioned in Fig. 8, the thermal energy is higher when symmetrical boundary conditions applied on both sides of the PV/T module for the channels located in the middle of the PV/T module. It is worth it to point out that nine channels out of eleven have symmetrical thermal boundary conditions (Sym. - Sym. B.C.) on both sides of the PV/T numerical model. While the channel on the lift side edge of the PV/T module has convection and symmetrical (Conv. - Sym. B.C.) thermal boundary conditions on the left and right sides edges of the PV/T numerical model, respectively, and vice versa for the right side edge of the PV/T module. The thermal energy variation with all values of mass flow rates for different thermal boundary conditions at 700 W/m^2 is shown in Fig. 9 (b). The thermal energy for both boundary conditions increases as the mass flow rates increase from 0.4 to 5.4 L/min. The big variation of thermal energy with the mass flow rates is clearly obtained for the channel in the middle of the PV/T module at the low mass flow rate as compared to the two channels on the left and right edges of the PV/T module. The total thermal energy for the PV/T model will follow the trend of thermal energy for symmetrical-symmetric boundary conditions, that because this boundary condition applied for the majority of channels (9 channel out of 11).

3.3.3. Three-dimensional temperature distribution

Fig. 10 shows the three-dimensional temperature distribution for the PV/T module. The temperature readings have the highest value at the upper surface where the PV/T module exposed to constant irradiance (heat flux). The temperature on the top surface increases along the direction of the cooling from the inlet at 334.8 K–342 K in the middle then tends to decrease again to 337.2 K at the outlet. The figure shows also the effect of symmetric-symmetric and symmetric convection boundary conditions on the temperature values. All the edges around the top side of the PV/T module, especially at the corners, where the symmetric convection boundary conditions applied have the lowest temperatures. The temperature of the PV/T module decreases from 334.8 to 342 K at the top surface to around 327.7 K at the middle plane between the top and bottom surfaces. The temperature reaches the lowest value of 311 K at the bottom surface where the water cooling channels installed.

3.3.4. Thermal efficiency of the PV/T system

The thermal efficiency under different irradiance and mass flow rates are displayed in Fig. 11 (a) and (b). Evidently, the thermal efficiency increases as the irradiance increase under the same mass

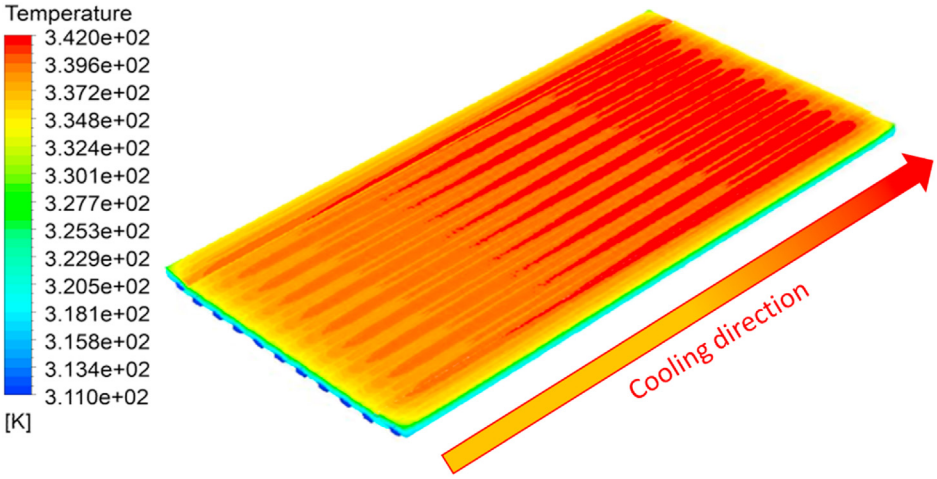

Fig. 10. Three-dimensional temperature distribution in (K) for PV/T system for a typical day in April in UAE.

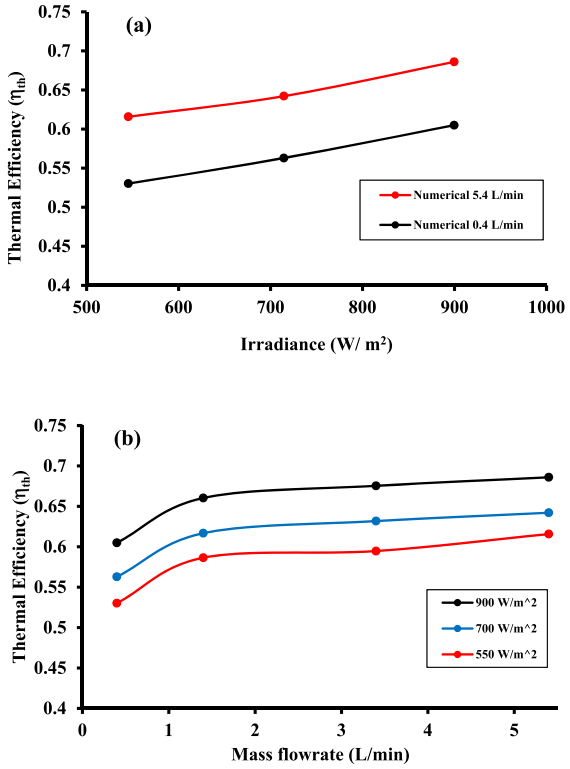

Fig. 11. Thermal efficiency for a typical day of April in UAE at **(a)** different irradiance values along the day **(b)** different values of mass flow rates.

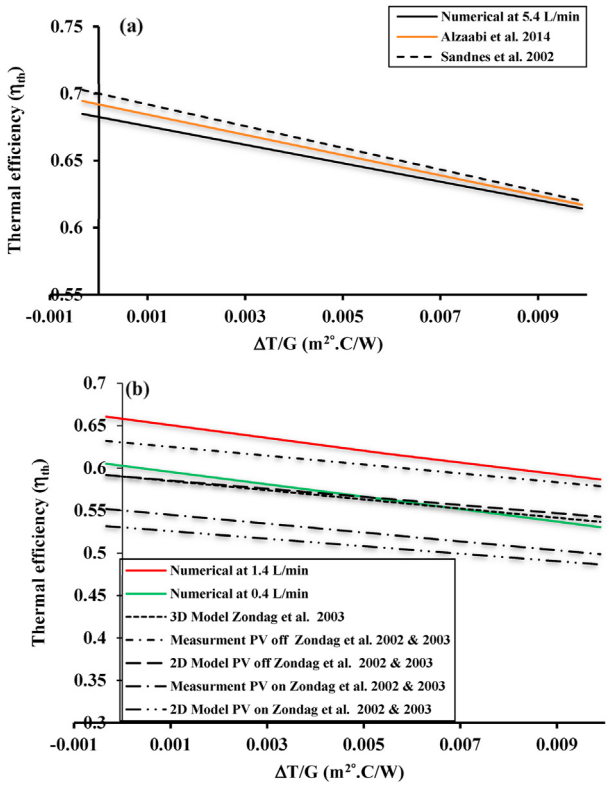

Fig. 12. Comparison of experimental and numerical thermal efficiency versus ΔT/G **(a)** at 5.4 L/min with work done by [39,44] **(b)** at 0.4 & 1.4 L/min with work done by [45,46].

flow rate, the mass flow rate 5.4 L/min has a higher thermal efficiency value than the mass flow rate 0.4 L/min, where the maximum η_{th} obtained at 900 (W/m^2) as displayed in Fig. 11 (a). Fig. 11 (b) shows the variation of the thermal efficiency with the mass flow rate. For 900 W/m^2, as the mass flow rate increases from 0.4 to 1.4 L/min the thermal efficiency increases from 61% to 66%. After that, it increases slightly from 66% to 69% as the mass flow rate increases from 1.4 to 5.4 L/min. It is noteworthy to mention that the feasible value of the mass flow rate in this study is 1.4 L/min. The feasible value of the mass flow rate is crucial for selecting the capacity of the pump which is an essential factor for the cost-effectiveness of the PV/T cooling system.

3.3.5. *Validation and verification of the current PV/T model*

The results of the thermal efficiency for this work were compared with several studies in the literature. For example, the numerical simulation of this work was performed for three different values of irradiance (500, 700, and 900 W/m^2) and four different mass flow rates (0.4, 1.4, 3.4, and 5.4 L/min). The removal factor $F_R(\tau\alpha)$ is the maximum efficiency that the PV/T module can achieve when ΔT/G equals zero, i.e. intersection of the vertical axis for η_{th} versus ΔT/G. The $F_R(\tau\alpha)$ computed from this numerical model was very close to the value reported in Sandnes et al., 2002 [59] at 5.4 (L/min). Moreover, the F_RU_L values have small differences due to the difference in the area of the PV module, evident from Fig. 12 (a) and Table 7. Furthermore, the values of $F_R(\tau\alpha)$ and F_RU_L reported in Sandnes et al., 2002 [59] depend on the weather conditions. On the other hand, the values of $F_R(\tau\alpha)$ and F_RU_L computed by the developed model at a low mass flow rate (0.4 and 1.4 L/min) were compared to the values reported in Tiwari et al., 2006 [58], Zondag et al., 2003 and 2002 [60,61] and Tripanagnostopoulos et al., 2002 [62], see Fig. 12 (b) and Table 2. However, the small difference in the values of F_RU_L is due to the difference in the PV module area and the high thermal conductivity of the copper cooling channel. It is evident from Table 2 that the values of F_RU_L for this work were high at low mass flow rates and were low at high mass flow rates.

Table 7 shows a summary of the results reported in the literature [58–62] for $F_R(\tau\alpha)$ and F_RU_L compared to the results obtained in this work for different PV/T module areas. The results reported in the literature were based on experimental work or numerical models of one, two, or three dimensional. Fig. 12, on the other hand, shows a comparison between the thermal efficiency in this study and various studies in the literature under varying values of ΔT/G for high and low mass flow rates. It is clear from Fig. 9 that the thermal efficiency is inversely proportional to ΔT/G for all studies. It is worth it to mention that the highest thermal efficiency obtained at different values of the mass flow rate [63–69], and the covered or glazed PV/T has less thermal efficiency compared with the uncovered or unglazed [59,60]. Moreover, in addition to mass flow rate value, the highest value of thermal efficiency for the PV/T system depends on many parameters such as ambient, operating conditions, the spacing between the channels, and the area of PV/T module as shown in Eqs. (6) and (7).

Table 7
Summary of thermal efficiency parameters (intersection *FR* ($\tau\alpha$), and slope F_RU_L) for the current work and other studies in the literature.

$\eta_{th\ at\ \Delta T/G=0}$ (%) or F_R ($\tau\alpha$)/average	F_RU_L (W/m^2.C)	Area (m^2)	Mass flow rate (Unit)	Irradiance (W/m^2)	Reference
0.70	8.10	0.32	–	–	[59]
0.6825	6.89	0.784	5.4 L/min		**[This study]**
0.72	8.50	0.32	–	–	[59]
0.6825	6.89	0.784	5.4 L/min		**[This study]**
0.58 (m PV off)	5.2	0.94	76 kg/m^2 h	800	[60]
0.63 (2D PV off)	4.8				
0.6575	7.24	0.784	1.4 L/min	550, 700 and 900	**[This study]**
0.53 (m PV on)	5.2				
0.55 (2D PV on)	4.4				
0.625/0.56 (1D)	5.4	0.94	0.02 kg/s	800	[61]
0.62/0.535 (2D)	4.8				
0.59 (3D)					
0.6575	7.24	0.784	1.4 L/min	550, 700 and 900	**[This study]**
0.71	9.04	0.4	0.02 kg/s	850.910, 898	[22]
0.6575	7.24	0.784	1.4 L/min	550, 700 and 900	**[This study]**
77.25		0.648	45 kg	Winter	[58]
60–65					
60.3–65.8	7.27	0.784	0.4–1.4 L/min	Summer	**[This study]**

4. Conclusions

Novel 3-D numerical simulations were performed under different irradiance conditions and mass flow rates to study the performance of the PV/T system. The computational time for numerical simulation was reduced by applying different thermal boundary conditions on both sides of the novel PV/T numerical model. The number of elements for the numerical simulations conducted in the literature was higher than the current study by 5–12 times which lead to an increase in the computational time. The current model is much simpler and more efficient with less computational time. The results demonstrate that the middle of the PV/T module has the highest temperature where the symmetrical boundary conditions were applied on both sides of the PV/T numerical model. Several factors, namely, the overall heat transfer coefficient, the mass flow rate, the area of PV module, the specific heat, and the ambient conditions (irradiance, ambient, and fluid cooling temperature) affect the thermal efficiency of the PV/T system. A low value of (ΔT/G) has the highest thermal efficiency where the irradiance and the temperature difference between the ambient temperature and the inlet temperature of the cooling fluid were very high and very low, respectively. The novel numerical model shows that these results were in a decent concurrence with the results reported in the literature. The overall efficiency enhanced not only by increasing the electrical efficiency from 1 to 1.5% but also by utilizing the thermal energy for some applications such as solar heating and cooling systems. As in solar liquid desiccant cooling system for trigeneration applications (cooling, heating, and power generation), solar desiccant wheel evaporative cooling system (SDWECS), adsorption gas heat pump, and domestic hot water. There are several limitations for this model such as the cooling channels were distributed in a symmetrical configuration, the cooling channels should be rectangular and fixed at the backside of the PV module, the contact region between the PV module and the cooling channels was assumed to be perfect without any resistance, the flow is incompressible and turbulent, and the variation on the wind speed is less than 4 m/s.

CRediT authorship contribution statement

Tareq Salameh: Conceptualization, Project administration, Methodology, Funding acquisition, Supervision, Writing - review & editing. **Muhammad Tawalbeh:** Investigation, Validation, Methodology, Formal analysis, Data curation, Writing - original draft. **Adel Juaidi:** Investigation, Methodology, Formal analysis, Writing - review & editing. **Ramez Abdallah:** Investigation, Methodology, Writing - review & editing. **Abdul-Kadir Hamid:** Project administration, Funding acquisition, Supervision, Writing - review & editing.

Declaration of competing interest

The authors declare that they have no known competing financial interests or personal relationships that could have appeared to influence the work reported in this paper.

Acknowledgement

The authors would like to acknowledge the: University of Sharjah and An Najah National University for facilitating this research.

References

[1] A. Ahmadi, M. El Haj Assad, D.H. Jamali, R. Kumar, Z.X. Li, T. Salameh, M. Al-Shabi, M.A. Ehyaei, Applications of geothermal organic Rankine Cycle for electricity production, J. Clean. Prod. 274 (2020) 122950.
[2] A.H. Alami, A. Abu Hawili, M. Tawalbeh, R. Hasan, L. Al Mahmoud, S. Chibib, A. Mahmood, K. Aokal, P. Rattanapany, Materials and logistics for carbon dioxide capture, storage and utilization, Sci. Total Environ. 717 (2020) 137221.
[3] C. Ghenai, T. Salameh, A. Merabet, Technico-economic analysis of off grid solar PV/Fuel cell energy system for residential community in desert region, Int. J. Hydrogen Energy 45 (2020) 11460–11470.
[4] A. Juaidi, F.G. Montoya, J.A. Gázquez, F. Manzano-Agugliaro, An overview of energy balance compared to sustainable energy in United Arab Emirates, Renew. Sustain. Energy Rev. 55 (2016) 1195–1209.
[5] R. Abdallah, A. Juaidi, S. Abdel-Fattah, F. Manzano-Agugliaro, Estimating the optimum tilt angles for south-facing surfaces in Palestine, Energies 13 (3) (2020) 623, https://doi.org/10.3390/en13030623.
[6] M.A. Ehyaei, A. Ahmadi, M. El Haj Assad, Tariq Salameh, Optimization of parabolic through collector (PTC) with multi objective swarm optimization (MOPSO) and energy, exergy and economic analyses, J. Clean. Prod. 234 (2019) 285–296.
[7] C. Ghenai, A. Merabet, T. Salameh, E.C. Pigem, Grid-tied and stand-alone hybrid solar power system for desalination plant, Desalination 435 (2018) 172–180.
[8] C. Ghenai, T. Salameh, A. Merabet, A.K. Hamid, Modeling and optimization of hybrid solar-diesel-battery power system, in: 7th International Conference on Modeling, Simulation, and Applied Optimization (ICMSAO), IEEE; (2017), 2017, pp. 1–5.
[9] M. Farshchimonfared, J.I. Bilbao, A.B. Sproul, Channel depth, air mass flow rate and air distribution duct diameter optimization of photovoltaic thermal (PV/T) air collectors linked to residential buildings, Renew. Energy 76 (2015) 27–35.

[10] A.H. Alami, K. Aokal, D. Zhang, M. Tawalbeh, A. Alhammadi, A. Taieb, Assessment of Calotropis natural dye extracts on the efficiency of dye-sensitized solar cells, Agron. Res. 16 (2018) 1569–1579.
[11] F. Schiro, A. Benato, A. Stoppato, N. Destro, Improving photovoltaics efficiency by water cooling: modelling and experimental approach, Energy 137 (2017) 798–810.
[12] J. Siecker, K. Kusakana, B.P. Numbi, A review of solar photovoltaic systems cooling technologies, Renew. Sustain. Energy Rev. 79 (2017) 192–203.
[13] S.S. Joshi, A.S. Dhoble, Photovoltaic -Thermal systems (PVT): technology review and future trends, Renew. Sustain. Energy Rev. 92 (2018) 848–882.
[14] C. Lamnatou, D. Chemisana, Photovoltaic/thermal (PVT) systems: a review with emphasis on environmental issues, Renew. Energy 105 (2017) 270–287.
[15] M.S. Buker, B. Mempouo, S.B. Riffat, Performance evaluation and techno-economic analysis of a novel building integrated PV/T roof collector: an experimental validation, Energy Build. 76 (2014) 164–175.
[16] F. Yazdanifard, E. Ebrahimnia-Bajestan, M. Ameri, Investigating the performance of a water-based photovoltaic/thermal (PV/T) collector in laminar and turbulent flow regime, Renew. Energy 99 (2016) 295–306.
[17] E. Bellos, C. Tzivanidis, Yearly performance of a hybrid PV operating with nanofluid, Renew. Energy 113 (2017) 867–884.
[18] R. Nasrin, N.A. Rahim, H. Fayaz, M. Hasanuzzaman, Water/MWCNT nanofluid based cooling system of PVT: experimental and numerical research, Renew. Energy 121 (2018) 286–300.
[19] A. Aldawoud, T. Salameh, Y.K. Kim, Double Skin Façade: Energy Performance in the United Arab Emirates, Energy Sources, Part B: Economics, Planning, and Policy, 2020. DOI.org/10.1080/15567249.2020.1813845.
[20] T. Salameh, M. El Haj Assad, M. Tawalbeh, C. Ghenai, A. Merabet, H.F. Öztop, Analysis of cooling load on commercial building in UAE climate using building integrated photovoltaic façade system, Solar Energy 199 (2020) 617–629.
[21] T. Salameh, C. Ghenai, A. Merabet, M. Alkasrawi, Techno-economical optimization of an integrated stand-alone hybrid solar PV tracking and diesel generator power system in Khorfakkan, United Arab Emirates, Energy 190 (2020) 116475.
[22] M.M. Aman, K.H. Solangi, M.S. Hossain, A. Badarudin, G.B. Jasmon, H. Mokhlis, A.H.A. Bakar, S. N Kazi, A review of Safety, Health and Environmental (SHE) issues of solar energy system, Renew. Sustain. Energy Rev. 41 (2015) 1190–1204.
[23] A.H. Alami, M. Faraj, K. Aokal, A.A. Hawili, M. Tawalbeh, D. Zhang, Investigating various permutations of copper iodide/FeCu tandem materials as electrodes for dye-sensitized solar cells with a natural dye, Nanomaterials 10 (4) (2020) 784, https://doi.org/10.3390/nano10040784.
[24] T. Salameh, M. Tawalbeh, A.H. Alami, A. Al-Othman, S. Issa, M. Alkasrawi, Life cycle analysis comparison between single crystalline solar cells and poly crystaline gallium in UAE, in: Advances in Science and Engineering Technology International Conferences (ASET): Dubai, United Arab Emirates (2020), 2020, pp. 1–6, https://doi.org/10.1109/ASET48392.2020.9118328.
[25] P. Bhubaneswari, S. Iniyan, R. Goic, A review of solar photovoltaic technologies, Renew. Sustain. Energy Rev. 15 (2011) 1625–1636.
[26] V. Eveloy, T. Gebreegziabher, Excess electricity and power-to-gas storage potential in the future renewable-based power generation sector in the United Arab Emirates, Energy 166 (2019) 426–450.
[27] M. Tawalbeh, T. Salameh, M. Albawab, A. Al-Othman, M.E.H. Assad, A.H. Alami, Parametric study of a single effect lithium bromide-water absorption chiller powered by a renewable heat source, Journal of Sustainable Development of Energy, Water and Environment Systems 8 (2020) 464–475.
[28] A. Al-Othman, M. Tawalbeh, M. El Haj Assad, T. Alkayyali, Eisa Ahmed, Novel multi-stage flash (MSF) desalination plant driven by parabolic trough collectors and a solar pond: a simulation study in UAE, Desalination 443 (2018) 237–244.
[29] V. Perraki, G. Tsolkas, Temperature dependence on the photovoltaic properties of selected thin-film modules, Int. J. Renew. Sustain. Energy 2 (2013) 140–146.
[30] M. Berginc, U.O. Krasovec, M. Jankovec, M. Topic, The effect of temperature on the performance of dye-sensitized solar cells based on a propyl-methyl-imidazolium iodide electrolyte, Sol. Energy Mater. Sol. Cells 91 (2007) 821–828.
[31] M. Mani, R. Pillai, Impact of dust on solar photovoltaic (PV) performance: research status, challenges and recommendations, Renew. Sustain. Energy Rev. 14 (2010) 3124–3131.
[32] F. Mejia, J. Kleissl, J.L. Bosch, The effect of dust on solar photovoltaic systems, Energy Procedia 49 (2014) 2370–2376.
[33] M.A. Green, S.P. Bremner, Energy conversion approaches and materials for high-efficiency photovoltaics, Nat. Mater. 16 (2017) 23–34.
[34] E. Skoplaki, J.A. Palyvos, On the temperature dependence of photovoltaic module electrical performance: a review of efficiency/power correlations, Sol. Energy 83 (2009) 614–624.
[35] R. Kumar, M.A. Rosen, A critical review of photovoltaic–thermal solar collectors for air heating, Appl. Energy 88 (2011) 3603–3614.
[36] S. Chander, A. Purohit, A. Sharma, S.P. Nehra, M.S. Dhaka, Impact of temperature on performance of series and parallel connected mono-crystalline silicon solar cells, Energy Rep. 1 (2015) 175–180.
[37] M. Al-Chaderchi, K. Sopian, T. Salameh, D. Zhang, M. Alghoul, Enhancing the performance of PV panel undergoing shading effects, Int. J. Power Electron. Drive Syst. 9 (2018) 937–1943.
[38] M. Al-chaderchi, K. Sopain, M. Alghoul, T. Salameh, Experimental study of the effect of fully shading on the Solar PV module performance, E3S Web of Conferences: EDP Sciences (2017), 01001.
[39] A.K. Tossa, Y.M. Soro, L. Thiaw, Y. Azoumah, L. Sicot, D. Yamegueu, C. Lishou, Y. Coulibaly, G. Razongles, Energy performance of different silicon photovoltaic technologies under hot and harsh climate, Energy 103 (2016) 261–270.
[40] S.A. Kalogirou, Y. Tripanagnostopoulos, Hybrid PV/T solar systems for domestic hot water and electricity production, Energy Convers. Manag. 47 (2006), 3368-3362.
[41] P. Ooshaksaraei, K. Sopian, S.H. Zaidi, R. Zulkifli, Performance of four air-based photovoltaic thermal collectors configurations with bifacial solar cells, Renew. Energy 102 (2017) 279–293.
[42] O. Rejeb, H. Dhaou, A. Jemni, A numerical investigation of a photovoltaic thermal (PV/T) collector, Renew. Energy 77 (2015) 43–50.
[43] R. Nasrin, M. Hasanuzzaman, N.A. Rahim, Effect of high irradiation and cooling on power, energy and performance of a PVT system, Renew. Energy 116 (2018) 552–569.
[44] A.H.A. Al-Waeli, M.T. Chaichan, K. Sopian, H.A. Kazem, H.B. Mahoodd, A.A. Khadom, Modeling and experimental validation of a PVT system using nanofluid coolant and nano-PCM, Sol. Energy 177 (2019) 178–191.
[45] W. Pang, Q. Zhang, Y. Cui, L. Zhang, H. Yu, X. Zhang, Y. Zhang, H. Yan, Numerical simulation and experimental validation of a photovoltaic/thermal system based on a roll-bond aluminum collector, Energy 187 (2019) 115990.
[46] S. Misha, A.L. Abdullah, N. Tamaldin, M.A.M. Rosli, F.A. Sachit, Simulation CFD and experimental investigation of PVT water system under natural malaysian weather conditions, Energy Reports (2019), https://doi.org/10.1016/j.egyr.2019.11.162. In press.
[47] T. Salameh, M. Tawalbeh, A. Juaidi, R. Abdallah, S. Issa, A.H. Alami, A novel numerical simulation model for the PVT water system in the GCC region, in: Advances in Science and Engineering Technology International Conferences (ASET): Dubai, United Arab Emirates (2020), 2020, pp. 1–5, https://doi.org/10.1109/ASET48392.2020.9118264.
[48] A.A. Alzaabi, N.K. Badawiyeh, H.O. Hantoush, A.K. Hamid, Electrical/thermal performance of hybrid PV/T system in Sharjah, UAE, International Journal of Smart Grid and Clean Energy 3 (2014) 385–389.
[49] C.C. Smith, T.A. Weiss, Design application of the Hottel-Whillier-Bliss equation, Sol. Energy 19 (2) (1977) 109–113.
[50] J. Yao, H. Xu, Y. Dai, M. Huang, Performance analysis of solar assisted heat pump coupled with build-in PCM heat storage based on PV/T panel, Sol. Energy 197 (2020) 279–291.
[51] J. Yao, W. Liu, Lu Zhang, Binshou Tian, Yanjun Dai, Mingjun Huang, Performance analysis of a residential heating system using borehole heat exchanger coupled with solar assisted PV/T heat pump, Renew. Energy 160 (2020) 160–175.
[52] L. de Santoli, G.L. Basso, B. Nastasi, The potential of hydrogen enriched natural gas deriving from power-to-gas option in building energy retrofitting, Energy Build. 149 (2017) 424–436.
[53] S.J. Kline, F.A. McClintock, Describing uncertainties in single-sample experiments, Mech. Eng. 75 (1953) 3–8.
[54] D.J. Yang, Z.F. Yuan, P.H. Lee, H.M. Yin, Simulation and experimental validation of heat transfer in a novel hybrid solar panel, Int. J. Heat Mass Tran. 55 (2012) 1076–1082.
[55] J.H. Watmuff, W.W.S. Charters, D. Proctor, Solar and Wind Induced External Coefficients - Solar Collectors, Cooperation Mediterraneenne Pour l'Energie Solaire, Revue Internationale d'Heliotechnique, 2nd Quarter, 1977, p. 56.
[56] I.B. Celik, U. Ghia, P.J. Roache, C.J. Freitas, Procedure for estimation and reporting of uncertainty due to discretization in CFD applications, ASME. J. Fluids Eng. July 130 (7) (2008), 078001.
[57] S. Armstrong, W.G. Hurley, A thermal model for photovoltaic panels under varying atmospheric conditions, Appl. Therm. Eng. 30 (2010) 1488–1495.
[58] A. Tiwari, M.S. Sodha, Performance evaluation of hybrid PV/thermal water/air heating system: a parametric study, Renew. Energy 31 (2006) 2460–2474.
[59] B. Sandnes, J. Rekstad, A photovoltaic/thermal (PV/T) collector with a polymer† absorber plate. Experimental study and analytical model, Sol. Energy (2002) 63–73.
[60] H.A. Zondag, D.W. de Vries, W.G.J. van Helden, R.J.C. van Zolingen, A.A. van Steenhoven, The yield of different combined PV-thermal collector designs, Sol. Energy 74 (2003) 253–269.
[61] H.A. Zondag, D.W. de Vries, W.G.J. van Helden, R.J.C. van Zolingen, A.A. van Steenhoven, The thermal and electrical yield of a PV-thermal collector, Sol. Energy 72 (2002) 113–128.
[62] Y. Tripanagnostopoulos, Th Nousia, M. Souliotis, P. Yianoulis, Hybrid photovoltaic/thermal solar systems, Sol. Energy 72 (2002) 217–234.
[63] T.T. Chow, Performance analysis of photovoltaic–thermal collector by explicit dynamic model, Sol. Energy 75 (2003) 143–152.
[64] Y. Morita, T. Fujisawa, T. Tani, Moment performance of photovoltaic/thermal hybrid panel (numerical analysis and exergetic evaluation), IEEE Trans. Ind. Appl. 199 (1999) 81–87.
[65] S.A. Kalogirou, Use of TRNSYS for modelling and simulation of a hybrid PV–thermal solar system for Cyprus, Renew. Energy 23 (2001) 247–260.
[66] J. Gao, Y. Zhang, Y. Liu, X. Gao, Study on the temperature variation of the water-cooled photovoltaic solar template, in: International Conference on Intelligent System Design and Engineering Application, IEEE, Changsha, China, 2010, 2010.
[67] T. Nualboonrueng, P. Tuenpusa, Y. Ueda, A. Akisawa, The performance of PV-T systems for residential application in Bangkok, Progress in Photovoltaics 21

(2013) 1204–1213.
[68] H.P. Garg, R.K. Agarwal, Some aspects of a PV/T collector/forced circulation flat plate solar water heater with solar cells, Energy Convers. Manag. 36 (1995) 87–99.
[69] J. Ji, J. Han, T. Chow, H. Yi, J. Lu, W. He, W. Sun, Effect of fluid flow and packing factor on energy performance of a wall mounted hybrid photovoltaic/water-heating collector system, Energy Build. 38 (2006) 1380–1387.